Open fires in Greenland in summer 2017: transport and deposition of BC and impact on the Greenland Ice Sheet

Nikolaos Evangeliou[1,*], Arve Kylling[1], Sabine Eckhardt[1], Viktor Myroniuk[2], Kerstin Stebel[1], Ronan Paugam[3], Sergiy Zibtsev[2], Andreas Stohl[1]

[1]Norwegian Institute for Air Research (NILU), Department of Atmospheric and Climate Research (ATMOS), Kjeller, Norway.
[2]National University of Life and Environmental Sciences of Ukraine, Kiev, Ukraine.
[3]King's College London, London, United Kingdom.

* Corresponding author: N. Evangeliou (Nikolaos.Evangeliou@nilu.no)

Abstract

Highly unusual open fires burned in Western Greenland between 31 July and 21 August 2017, after a period of warm, dry and sunny weather. The fires burned on peat lands that became vulnerable to fires by permafrost thawing. We used several satellite data sets to estimate that the total area burned was about 2345 hectares. Based on assumptions of typical burn depths and BC emission factors for peat fires, we estimate that the fires consumed a fuel amount of about 117 kt C and produced BC emissions of about 23.5 t. We used a Lagrangian particle dispersion model to simulate the atmospheric BC transport and deposition. We find that the smoke plumes were often pushed towards the Greenland Ice Sheet by westerly winds and thus a large fraction of the BC emissions (7 t or 30%) was deposited on snow or ice covered surfaces. The calculated BC deposition was small compared to BC deposition from global sources, but not entirely negligible. Analysis of aerosol optical depth data from three sites in Western Greenland in August 2017 showed strong influence of forest fire plumes from Canada, but little impact of the Greenland fires. Nevertheless, CALIOP lidar data showed that our model captured the presence and structure of the plume from the Greenland fires. The albedo changes and instantaneous surface radiative forcing in Greenland due to the fire BC emissions were estimated with the SNICAR model and the uvspec model from the libRadtran radiative transfer software package. We estimate that the maximum albedo change due to the BC deposition was about 0.006, too small to be measured. The average instantaneous surface radiative forcing over Greenland at noon on 31 August was 0.03 W m^{-2}, with locally occurring maximum values of 0.63 W m^{-2}. The average value is at least an order of magnitude smaller than the radiative forcing due to BC from other sources. Overall, the fires burning in Greenland in summer of 2017 had little impact on BC deposition on the Greenland Ice Sheet, causing almost negligible extra radiative forcing. This was due to the – in a global context – still rather small size of the fires. However, the very large fraction of the BC emissions deposited on the Greenland Ice Sheet makes these fires very efficient climate forcers on a per unit emission basis. If the expected future warming of the Arctic produces more severe fires in Greenland, this could indeed cause albedo changes and thus contribute to accelerated melting of the Greenland Ice Sheet. The fires burning in 2017 may be a harbinger of such future events.

1 Introduction

In August 2017 public media reported unprecedented fire events in Western Greenland (BBC News, 2017; New Scientist Magazine, 2017). These events were documented with airborne photographs (SERMITSIAQ, 2017) and satellite images (NASA, 2017b) and raised public concerns about the effects of climate change and possible impacts of soot emissions on ice melting. Historically, wildfires have occurred infrequently on Greenland, because three-quarters of the island is covered by a permanent ice sheet and permafrost is found on most of the ice-free land (Abdalati and Steffen, 2001). Permafrost, or permanently frozen soil, lies under a several meters thick "active" soil layer that thaws seasonally. But in certain areas, where the permafrost layer starts melting, it can expose peat, a material consisting of only partially decomposed vegetation that forms in wetlands over the course of hundreds of years or longer. Peatlands, also known as bogs and moors, are the earliest stage in the formation of coal. Globally, the amount of carbon stored in peat exceeds that stored in vegetation and is similar in size to the current atmospheric carbon pool (Turetsky et al., 2014). When peatlands dry, they are often affected by fires burning into the peat layers. Peat fires are difficult to extinguish and they often burn until all the organic matter is consumed. Smoldering peat fires already are the largest fires on Earth in terms of their carbon footprint (Turetsky et al., 2014). For Greenland, it has been suggested that degradation of peat will accelerate towards 2080 (Daanen et al., 2011) and that the area affected by the fires in August 2017 is particularly vulnerable to permafrost thawing (Daanen et al., 2011).

Fires in the high northern latitudes release significant amounts of CO_2, CH_4, N_2O and black carbon (BC), and their emissions are often transported into Arctic regions (Cofer III et al., 1991; Hao et al., 2016; Hao and Ward, 1993; Shi et al., 2015). BC is the most strongly light-absorbing component of the atmospheric aerosol (Bond et al., 2013) and is formed by the incomplete combustion of fossil fuels, biofuels, and biomass. It is important due to its human health (Lelieveld et al., 2015) and climate impacts (Sand et al., 2015), and its atmospheric lifetime of 3–11 days (Bond et al., 2013) facilitates transport over long distances (Forster et al., 2001; Stohl et al., 2006). BC from mid-latitude sources can thus reach remote areas such as the Arctic. BC absorbs solar radiation in the atmosphere and has a significant impact on cloud formation. It also decreases surface albedo when deposited on ice and snow and can accelerate melting processes (Hansen and Nazarenko, 2004). This raises particular concerns about the effect of fires burning in the immediate vicinity of the Greenland Ice Sheet. If a large fraction of the BC emitted by such fires is deposited on the ice, these fires may be extremely effective in further enhancing the already accelerating melting of the Greenland Ice Sheet (AMAP, 2017). BC emissions from such high latitude fires may also have a substantial effect on the albedo of sea ice.

Here we study transport and deposition of BC over the Greenland Ice Sheet from the fires that occurred in Western Greenland in August 2017, which likely represent the largest fires that have occurred on Greenland in modern times (Figure S 1). Since the fires occurred in an area entirely lacking ground-based observations, we use satellite data and a Lagrangian atmospheric dispersion model for our study.

2 Methods

2.1 Definition of burned area

Remote sensing has been useful for delineating fire perimeters, characterizing burn severity and planning post-fire restoration activities in different regions. The use of satellite imaging is particularly important for fire monitoring in remote areas due to difficult ground access. The method that is presented in this section has been already used to calculate burned area in the highly-contaminated radioactive forests of Chernobyl (Evangeliou et al., 2014, 2015, 2016). Coordinates of fire locations (hot spots) were downloaded from FIRMS (Fire Information for Resource Management System) (NASA, 2017a). For the mapping of the burned area, Sentinel 2A images were used. To delineate fire perimeters and define burn severity precisely, we used Landsat 8 Operational Land Imager (OLI) (resolution: 30×30 m) together with Sentinel 1A (resolution: 30×30 m) and Sentinel 2A images (resolution: 30×30 m) (see Table 1) by applying the differenced Normalized Burn Ratio (dNBR) (Key and Benson, 2006):

$$dNBR = NBR_{pre-fire} - NBR_{post-fire} \qquad \text{(Eq. 1)}$$

Normalized burn ratios for pre- ($NBR_{pre-fire}$) and postfire ($NBR_{post-fire}$) images from Sentinel 2A can be calculated using radiances for near- and shortwave infrared bands (bands 8 (NIR) and 12 (SWIR2) at 0.835 µm and 2.202 µm, respectively):

$$NBR = \frac{1000 \cdot (NIR - SWIR2)}{NIR + SWIR2} \qquad \text{(Eq. 2)}$$

The methodology of applying a dNBR index to assess the impact of fires has been used in forests of the Northern and Western USA (French et al., 2008; Key and Benson, 2006) and elsewhere (Escuin et al., 2008; Sunderman and Weisberg, 2011).

The burned severity mosaics were created using Sentinel 2A images corrected for atmospheric scattering (see Chavez, 1988). Pre– and post–fire images were used to create cloudless mosaics for the area where the Greenland fires burned. A Maximum Value Composite (MVC) procedure (Holben, 1986) was used to select pixels from each band that were not cloud covered and have a high value of Normalized Difference Vegetation Index (NDVI). To avoid spurious burn severity values, manually delineated fire perimeters were applied and all areas outside were classified as unburned. We have used common dNBR severity levels (Key and Benson, 2006) that are presented in Figure 1. The occasionally dense cloud cover was the main obstacle in reconstructing fire dynamics. As an independent source of information, active fires from MODIS satellite product MCD14DL (Giglio et al., 2003) are plotted in Supplemental Information (SI) Figure S 2.

2.2 Injection altitudes, assumptions on biomass consumption and emissions factors

Injection heights into the atmosphere of the emitted smoke were simulated with version 2 of the Plume Rise Model (PRM) (Paugam et al., 2015) which is implemented in the Global Fire Assimilation System (GFAS) emission inventory (Rémy et al., 2017). The model (hereafter referred to as PRMv2) is a further development of PRM (Freitas et al., 2006, 2010) and has already been used in previous studies of fire events (Evangeliou et al., 2015, 2016). The model simulates a profile of smoke detrainment for every single fire, from which two metrics are extracted: (i) a detrainment layer (i.e. where the detrainment rate is > 50% of its global maximum) and (ii) an injection height (InjH, the top of the detrainment layer). Instead of using the GFAS product, which uses the same statistics as in the PRMv2 InjH calculation, we ran the model for every detected fire assuming a 6 h persistence and using the same conversion factor as Kaiser et al. (2012) to estimate the biomass consumption. PRMv2 mass detrainment profiles are then time integrated and extracted at 1°×1° spatial resolution with a 500 m vertical mesh to estimate the 3D distribution of biomass burning smoke injection into the atmosphere. Figure S 3 (SI) shows for all fires recorded in the MODIS fire product (Justice et al., 2002) during the fire period (31 July – 21 August 2017) the horizontal distribution of the median height of the emitted smoke and its integration over the longitude (right panel). Fires in Greenland showed a maximum injection height of around 2 km, but according to PRMv2 the majority of the emissions (90%) remained below 800 m. Low injection heights mostly inside the daytime planetary boundary layer are quite typical for smoldering fires including peat fires (Ferguson et al., 2003) such as those burning in

Greenland (see below). For modeling the dispersion of BC released from the Greenland fires, the emission profiles from PRMv2 were ingested into the Lagrangian particle dispersion model FLEXPART (see section 2.3).

Wildfires in boreal peatlands in the Canadian Arctic and in Alaska typically have (shallow) burn depths of 1–10 cm and consume 20–30 t C ha^{-1} (Benscoter and Wieder, 2003; Shetler et al., 2008). The consumed carbon is often re-sequestered in 60–140 years after the fire (Turetsky et al., 2011; Wieder et al., 2009). Given that fire return intervals can be as short as 100–150 years in sub-humid continental peatlands (Wieder et al., 2009), and may exceed 2000 years in humid climates (Lavoie and Pellerin, 2007), northern peatlands are generally resilient to wildfire (Magnan et al., 2012). For example, in peatlands of Northern Russia, organic matter available for combustion has been estimated to be 121.8 t C ha^{-1} for forested lands and 21.3 t C ha^{-1} for non-forested lands (Smirnov et al., 2015). Accordingly, a severe wildfire that burned within an afforested peatland in the Scottish Highlands during the summer of 2006 had a mean depth of burn of 17.5±2.0 cm (range: 1–54 cm) and a carbon loss of 96±15 t C ha^{-1} (Davies et al., 2013). In contrast, tropical peatlands can have deep burn depths of 40–50 cm and release an average of 300–450 t C ha^{-1} (Page et al., 2015; Reddy et al., 2015). In the present study, we assume an average amount of organic fuel available for combustion for the Greenland peat fires of August 2017 of 100 t C ha^{-1}, guided by values suggested elsewhere (Smirnov et al., 2015).

Estimation of the emissions of BC, E_{BC} (kg), was based on the following formula (Seiler and Crutzen, 1980; Urbanski et al., 2011) using the calculated burned area A (ha) and a number of assumptions:

$$E_{BC} = A \times FL \times \alpha \times EF \qquad \text{Eq. 1}$$

Here, FL is the mass of the fuel available for combustion (kg C ha^{-1}); α is the dimensionless combustion completeness, which was adopted from Hao et al. (2016) for litter and duff fuels (50%) and EF is the emission factor of BC (kg kg^{-1}) that was adopted from Akagi et al. (2011) for peatland fires (0.0002 kg kg^{-1}). Fuel consumption is calculated as the product of burned area, fuel loading and combustion completeness ($A \times FL \times \alpha$).

2.3 Atmospheric modeling

The emissions of BC obtained from Eq. 1 were fed to the Lagrangian particle dispersion model FLEXPART version 10.2 (Stohl et al., 2005) to simulate BC transport and deposition. This model was originally developed for calculating the dispersion of radioactive material from nuclear emergencies, but since then it has been used for many other applications (e.g., Fang et al., 2014; Stohl et al., 2011, 2013). The model has a detailed description of particle dispersion in the boundary layer and a convection scheme to simulate particle transport in clouds (Forster et al., 2007). The model was driven by hourly 0.5°×0.5° operational analyses from the European Centre for Medium-Range Weather Forecasts (ECMWF). Concentration and deposition fields were recorded in a global domain of 1°×1° spatial resolution with three hourly outputs. To capture the spatiotemporal variability of BC over the Greenland Ice Sheet, a nested domain with 0.05°×0.05° resolution was used. The simulations accounted for wet and dry deposition, assuming a particle density of 1500 kg m^{-3} and a logarithmic size distribution with an aerodynamic mean diameter of 0.25 μm and a standard deviation of 0.3 (Long et al., 2013). The wet deposition scheme considers below-cloud and in-cloud scavenging separately based on cloud liquid water and cloud ice content, precipitation rate and cloud depth from ECMWF, as described in Grythe et al. (2017).

To compare BC concentrations in Greenland due to the emissions of the Greenland fires to those due to BC emissions occurring elsewhere, we used the so-called "retroplume" mode of FLEXPART for determining the influence of other sources. For only a few receptor points, this mode is computationally more efficient than forward simulations. Computational particles were tracked 30 days back in time from four receptor regions: Northwestern (-62°E to -42°E, 72°N to 83°N), Southwestern (-62°E to -42°E, 61°N to 72°N), Northeastern (-42°E to -17°E, 72°N to 83°N) and Southeastern Greenland (-42°E to -17°E, 61°N to 72°N). The retroplume mode allowed identification of the origin of BC through calculated footprint emission sensitivities (often also called source-receptor relationships) that express the sensitivity of the BC surface concentration at the receptor to emissions on the model output grid. If these emissions are known, the BC concentrations at the receptor can be calculated as the product of the emission flux and the emission sensitivity. Also, detailed source contribution maps can be calculated, showing which regions contributed to the simulated concentration. For the anthropogenic emissions, we used the ECLIPSE (Evaluating the CLimate and Air Quality ImPacts of ShortlivEd Pollutants) version 5 (Klimont et al., 2017) emission data set. For the biomass burning emissions outside Greenland, we used operational CAMS GFAS emissions (Kaiser et al., 2012).

2.4 Radiative forcing calculations

The radiative forcing (RF) of the emitted BC was calculated using the uvspec model from the libRadtran radiative transfer software package (http://www.libradtran.org/doku.php)

(Emde et al., 2016; Mayer and Kylling, 2005). The radiative transfer equation was solved in the independent pixel approximation using the DISORT model in pseudo-spherical geometry with improved treatment of peaked phase functions (Buras et al., 2011; Dahlback and Stamnes, 1991; Stamnes et al., 1988). Radiation absorption by gases was taken from the Kato et al. (1999) parameterization modified as described in the libRadtran documentation and Wandji Nyamsi et al. (2015). External mixture of aerosols was assumed, i.e. BC was treated in isolation of other aerosol types that may also have been present in the plume. This assumption likely leads to underestimates of the radiative impacts of BC in the atmosphere as coating, for example, can enhance the radiative effects of BC. However, these assumptions should have little impact on the more important albedo calculations (see below).For snow-covered surfaces, deposited BC was assumed to reside in the uppermost 5 mm. Below 5 mm the snow was assumed to be without any impurities. The albedo of the snow was calculated with the SNICAR model (http://snow.engin.umich.edu/info.html) in a two-layer configuration (Flanner et al., 2007, 2009).

We calculated both the bottom of the atmosphere (BOA) and top of atmosphere (TOA) instantaneous radiative forcing (IRF) due to the Greenland fires at 1°×1° resolution. The IRF includes both the effects of atmospheric BC and BC deposited on the snow. Note that the IRF does not include any semi-direct nor indirect effects. We also calculated IRF for both cloudless and cloudy conditions. IRF for cloudless conditions indicates the maximum possible effect of BC due to the fires irrespective of the actual meteorological situation, while IRF for cloudy conditions is representative of the actual conditions. For the latter, liquid and ice water clouds were adopted from ECMWF.

2.5 Remote sensing of the smoke plume

To confirm the presence of BC from fires in Greenland and elsewhere in the atmosphere over Greenland, we used the AERONET (AErosol RObotic NETwork) data (Holben et al., 1998). AERONET provides globally distributed observations of spectral aerosol optical depth (AOD), inversion products, and precipitable water in diverse aerosol regimes. We chose data from three stations that were close to the 2017 fires and for which cloud-free data exist for most of the simulated period, namely Kangerlussuaq (50.62°W–66.99°N), Narsarsuaq (45.52°W–61.16°N) and Thule (68.77°W–76.51°N). Their locations are shown in Figure S 2. We used Level 2.0 AOD data (fine and coarse mode AOD at 500 nm and total AOD at 400 nm) from the AERONET version 3 direct-sun spectral deconvolution algorithm (SDA version

4.1) product (downloaded on 20/06/2018) for the simulated period (31 July to 31 August 2017).

To examine in particular the vertical depth of the smoke, we used data from the CALIOP (Cloud-Aerosol Lidar with Orthogonal Polarization) lidar on the CALIPSO (Cloud-Aerosol Lidar and Infrared Pathfinder Satellite Observations) platform (Winker et al., 2009). CALIOP provides profiles of backscatter at 532 nm and 1064 nm, as well as the degree of the linear polarization of the 532 nm signal. For altitudes below 8.3 km lidar profiles at 532 nm are available with a vertical resolution of 30 m. We have utilized the level 1 data products (version 3.40) of total attenuated backscatter at 532 nm. This signal responds to aerosols (like BC) as well as water and ice clouds, which in most cases can be distinguished based on their differences in optical properties. The data were downloaded via ftp from the ICARE Data and Services Center (http://www.icare.univ-lille1.fr/).

3 Results

3.1 Indications of early permafrost degradation and fuel availability

Table 1 reports burned areas in August 2017 calculated for Greenland. In total, 2345 hectares burned between 31 July and 21 August 2017 (Figure 1). We estimate that about 117 kt of carbon were consumed by these fires. The area burned is not large compared to the global area burned each year of 464 million hectares, or the areas burned in boreal North America (2.6 million hectares) or boreal Asia (9.8 million hectares) (Randerson et al., 2012), but still highly unusual for Greenland.

It is not yet known how these fires started. Fires on carbon-rich soils can be initiated by an external source, e.g. lightning, flaming wildfire and firebrand, or self-heating. The fires burned relatively close to the town of Sisimut, so it is quite possible that humans started the fires. Self-heating is another possibility as porous solid fuels can undergo spontaneous exothermic reactions in oxidative atmospheres at low temperatures (Drysdale, 2011; Restuccia et al., 2017b). This process starts by slow exothermic oxidation at ambient temperature, causing a temperature increase, which is determined by the imbalance between the rate of heat generation and the rate of heat losses (Drysdale, 2011). Fire initiated by self-heating ignition is a well-known hazard for many natural materials (Fernandez Anez et al., 2015; Restuccia et al., 2017a; Wu et al., 2015) and can also occur in natural soils (Restuccia et al., 2017b). Southwestern Greenland was under anticyclonic influence during the last week of July and according to the MODIS ESDIS worldview tool, direct sunshine occurred for eight consecutive days before the fires started at the end of July 2017. It might be possible that this long period of almost continuous insolation at these latitudes in July heated the soil enough to self-ignite. In any case, the continuous sunshine had dried the soil, making it susceptible to fire.

The fact that these fires were burning for about three weeks but spread relatively slowly compared to above-ground vegetation fires indicates that the main fuel was probably peat. The predominant vegetation in Western Greenland varies from carbon-rich Salix glauca low shrubs (mean canopy height: 95 cm), mainly at low altitude south-facing slopes with deep soils and ample moisture, to dwarf-shrubs and thermophilous graminoid vegetation (Arctic steppe) at higher altitudes (Jedrzejek et al., 2013). In addition, the observed smoke was nearly white, indicating damp fuel, such as freshly thawed permafrost, which produces smoke rich in organic carbon (OC) aerosol (Stockwell et al., 2016). Notice that while OC is not strongly absorbing, it may contain some absorbing brown carbon, which would add to the albedo reduction of snow by BC. On the other hand, BC emission factors are relatively low for peat fires (see Akagi et al., 2011).

Literally no fires should be expected in Greenland, since there is little available fuel as it has been suggested by global models and validated by observations (Daanen et al., 2011; Stendel et al., 2008); the only way to provide substantial amounts of fuel in Greenland is permafrost degradation. However, it has been suggested that significant permafrost loss in Greenland may occur only by the end of the 21st century (Daanen et al., 2011; Stendel et al., 2008). The fires in 2017 might indicate that significant permafrost degradation has occurred sooner than expected.

3.2 Transport and deposition of BC in Greenland

We estimate that about 23.5 t of BC were released from the Greenland fires in August 2017 (Table 1). According to the FLEXPART model simulations, these emissions were transported and deposited as shown in Figure 2. Due to the low injection altitude of the releases within the boundary layer, transport was relatively slow and thus most BC initially remained quite close to its emission source. Slow transport was also favored by mostly anticyclonic influence during the first half of August. It seems that even though katabatic winds from the Greenland Ice Sheet occasionally transported the plume westwards, most of the time the large-scale circulation pushed the plume back towards Greenland. Consequently, a large fraction of the emitted BC was deposited in Southwestern Greenland. On 3 August a small portion of the emitted BC (≈516 kg) was lifted higher into the atmosphere and was transported to the east and deposited in the middle of the Ice Sheet over the course of the following two days (4 and 5 August). From 5 to 8 August, when the fires were particularly intense, BC was transported to the south, where most of it was deposited at the southern part of the Ice Sheet and close to the coastline. At the same time, another branch of the plume was moving to the north depositing BC over Greenland's western coastline up to 80°N. Around 10 August, the plume circulated north- and then eastwards in the northwestern sector of the anti-cyclone and BC was deposited to the northern part of the Ice Sheet until 13 August. From around 16 August, a cyclone approached from the northwest and the smoke was briefly transported directly eastwards along the southern edge of the cyclone. Strong rain associated with the cyclone's frontal system appears to have largely extinguished the fire by 17 or 18 August, although smaller patches may have continued smoldering for a few more days before they also died out. The exact fire behavior after 16 August is difficult to determine because of frequent dense cloud cover. However, satellite imagery on 21 August shows no smoke anymore in the area where the fires had burned.

The total deposition of BC from the fires in Greenland is shown in Figure 2b. About 9 t of the 23.5 t of BC emitted (or about 39%) were deposited over Greenland. About 7 t (30% of the total emissions) were deposited on snow or ice covered surfaces. Most of the rest was deposited in the Baffin Bay between Greenland and Canada and in the Atlantic Ocean.

With 30% of the emissions deposited on snow or ice surfaces, Greenland fires may have a relatively large efficiency for causing albedo changes on the Greenland Ice Sheet. By comparison, the respective BC deposition on snow and ice surfaces over Greenland from global emissions of BC was only 0.4% (39 kt) of the emissions. Even the total deposition of BC in the Arctic (>67°N) was only about 3% (215 kt). This indicates the high relative potential of Greenland fires to pollute the cryosphere (on a per unit emission basis), likely also giving them a particularly high radiative forcing efficiency. Considering that the projected rise of Greenland temperatures is expected to result in further degradation of the permafrost (Daanen et al., 2011) and, hence, likely resulting in more and larger peat fires on Greenland, this constitutes a potentially important climate feedback which could accelerate melting of the glaciers and ice sheet of Greenland and enhance Arctic warming.

We also calculated the concentration of the deposited BC in Greenland snow (Figure 3) by taking the ratio of deposited BC and the amount of water deposited by rain or snow fall during the same time period (31 July to 31 August 2017). As expected, BC snow concentrations show the same general patterns as the simulated deposition of BC with the highest concentrations obtained close to the source. High BC in snow concentrations were also computed in some regions of the Ice Sheet due to relatively intense precipitation events. By contrast, dry deposition of BC over the Ice Sheets was low (Figure 3). Dry deposition was responsible for a major fraction of the deposition only in regions where the plume was transported during dry weather, and in most of these regions total deposition was low. A notable exception is the region close to the fires, where dry deposition was relatively important due to the generally dry weather when the fires were burning. It can be also ascribed to the fact that dry deposition occurs in the quasi-laminar sub–layer close to the surface. A fraction of the aerosols can be quickly deposited close to the sources before the they are transported to higher altitudes and away from the sources (Bellouin and Haywood, 2014). The average calculated concentration of BC on the Ice Sheet was estimated to be <1 ng g^{-1}, but in some areas snow concentrations reached up to 3 ng g^{-1}. These higher values are substantial considering that measured concentrations of BC in snow typically range up to 16 ng g^{-1} in most of Greenland (Doherty et al., 2010) or from 1 – 17 ng g^{-1} in summer 2012 and 3–43 ng g^{-1} in summer 2013 (Polashenski et al., 2015) and up to 15 ppb (ng g^{-1}) during preindustrial times (from 1740 to 1870) on average (Legrand et al., 2016).

It has been reported that the size of rapidly coagulated BC particles produced by different types of fires ranges between 0.1 to 10 μm, but more than 90% of the BC mass lies between 0.1 and 1 μm (e.g., Conny and Slater, 2002; Long et al., 2013; Zhuravleva et al., 2017 and many others). Therefore, we have chosen to simulate the Greenland fires with an aerodynamic mean diameter of 0.25 μm for BC and a logarithmic standard deviation of 0.3 (see section 2.3). To examine the sensitivity of deposition of BC in the Greenland Ice Sheet from the Greenland fires of 2017 to the particle size distribution used in the model, we simulated the same event for BC particles with aerodynamic mean diameters of 0.1, 0.25, 0.5, 1, 2, 4 and 8 μm and calculated the relative standard deviation of the deposition of BC normalized against the aerodynamic mean diameter of 0.25 μm that was our basic assumption (Figure S 4). The use of different size distributions for the BC particles produced from the 2017 fires created a relative uncertainty on the deposited mass of BC in the Greenland Ice Sheet, which ranges from 10%–30% in 86% of the Sheet's surface to up to 50% in the rest of the Sheet's surface. As expected, the calculated uncertainty is sensitive to the use of larger particles for BC; though BC particles larger than 1 μm are rather rare in peat fires (Hosseini et al., 2010; Leino et al., 2014).

3.3 Impact from other emissions in Northern Hemisphere

In summertime 2017, intense wildfires were reported in British Columbia, Western Canada (NASA, 2017c), and fires also burned at mid latitudes in Eurasia, as is typical during spring and summer (Hao et al., 2016). Previous studies of wildfires have shown that the produced energy can be sufficient to loft smoke above the boundary layer by supercell convection (Fromm et al., 2005) even up to stratospheric altitudes (Leung et al., 2007). As a result, BC can become subject to long-range transport over long distances (Forster et al., 2001; Stohl et al., 2007). To examine the impact of these fires in Greenland, average footprint emission sensitivities were calculated for four compartments of Greenland (Northwestern, Southwestern, Northeastern and Southeastern Greenland) for the period 31 July to 31 August 2017 and the results are shown in Figure S 5 together with the active fires in the Northern Hemisphere from 10 July to 31 August 2017 adopted from the MODIS satellite product (MCD14DL) (Giglio et al., 2003). As can be seen in Figure S 5, fires in Alaska might have affected BC concentrations in Greenland, as the corresponding emission sensitivities are the highest in North America. On the contrary, BC emitted from fires in Eurasia seems to have affected Greenland less.

Using gridded emissions for BC, the contribution of both biomass burning and anthropogenic sources to surface BC concentrations in the four different regions over Greenland (Northwestern, Northeastern, Southwestern and Southeastern Greenland, Figure S 6) was calculated (see section 2.3). Fires affected the northern part of Greenland more than the southern part with an average concentration of about 30 ng m^{-3}, almost twice the respective average for Southern Greenland (≈16 ng m^{-3}). About one third of the BC originated from wildfires in Eurasia and the rest from North America where the year 2017 appears to have been a particularly high fire year. The anthropogenic contribution to surface BC over Greenland was only about 14% to 50% of the total contribution from all biomass burning sources (Figure S 6), similar to what has been suggested previously for the Arctic in summer (Winiger et al., 2017). The anthropogenic contribution is larger in Southern Greenland than in Northern Greenland, due to the shorter distance from the main emission areas of North America and Western Europe, but it remains lower than the biomass burning contribution. The BC concentrations that are calculated here for the studied fire period (31 July to 31 August 2017) are relatively high compared to those reported previously. For instance, von Schneidemesser et al. (2009) observed an annual average BC concentration of 20 ng m^{-3} at Summit (Greenland) in 2006, while Massling et al. (2015) reported a summer average BC concentration of 11 ng m^{-3} at station Nord (Greenland) between May 2011 and August 2013. We attribute this to more active fires during 2017 than in previous years.

To compare how important Northern Hemispheric biomass burning emissions were for the air over Greenland, we present time-series of surface BC concentrations in Northwestern, Northeastern, Southwestern and Southeastern Greenland from the fires in Greenland and from all the other wildfire emissions occurring outside Greenland (North Hemisphere) for the same period of time (Figure 4). The calculated dosages (concentrations summed over a specific time period) for the same time period were also computed. The fires in Greenland affected mainly its western part with concentrations that reached up to 4.8 ng m^{-3} (Southwestern Greenland on 10 August) and 4.4 ng m^{-3} (Northwestern Greenland on 12 August), while BC concentrations in the eastern part remained significantly lower (Figure 4). These concentrations are substantial considering that the observed surface BC concentrations in Greenland in summer are usually below 20 ng m^{-3} (Massling et al., 2015). Surface BC due to wildfires occurring outside Greenland was also low most of the time in the studied period (up to 10 ng m^{-3} at maximum) except for a large peak between 19 and 23 August that mainly affected Northern Greenland (Figure 4). The concentrations during this episodic peak were as high as 27 ng m^{-3}. During the same period, the contribution from anthropogenic emissions was also a few ng m^{-3} (Figure 4). BC dosages for the simulation period (31 July – 10 August 2017) in Western Greenland due to the Greenland fires were about one order of magnitude smaller than dosages from fires elsewhere but of the same order of magnitude as BC originating from anthropogenic emissions.

4 Discussion

4.1 A validation attempt

There are few observations available that can be used to validate our model results. We use the AERONET and CALIOP data for some qualitative comparisons. Contours of simulated vertical distribution of BC and column-integrated simulated BC from fires inside and outside Greenland are plotted together with time-series of measured AOD (fine and coarse mode AOD at 500 nm and total AOD at 400 nm) for the AERONET stations Kangerlussuaq, Narsarsuaq and Thule (Figure 5). It can be seen that observed AOD variations were in very good agreement with the variation of simulated column-integrated BC from fires outside Greenland (mainly in Canada), confirming that the transport of these fire plumes was well captured by FLEXPART. Good examples are the peaks at Kangerlussuaq on 24 August, at Narsarsuaq on 19 August and at Thule on 21 August (Figure 5) that are attributed to the Canadian fires. The simulated contribution of the Greenland fires to simulated BC burdens was negligible by comparison, except at Kangerlussuaq in the beginning of August when the Greenland fire emissions were the highest. This station is less than 100 km away from where the fires burned, but not in the main direction of the BC plume transport. It seems the period of simulated fire influence corresponds to a small increase of the observed AOD values of up to 20% (Figure 5).

To validate the smoke plume's vertical extent, we used the CALIOP data. These data were only available from 5 August 2017 onward and frequent dense cloud cover inhibited lidar observations at the altitudes below the clouds. High aerosol backscatter was only found in the close vicinity of the fires. Figure 6a shows NASA's ESDIS view of the plume on 14 August 2017 at 6 UTC (available: https://worldview.earthdata.nasa.gov/?p=geographic&l=MODIS_Aqua_CorrectedReflectance_TrueColor(hidden),MODIS_Terra_CorrectedReflectance_TrueColor,MODIS_Fires_Terra,MODIS_Fires_Aqua,Reference_Labels(hidden),Reference_Features,Coastlines&t=2017-08-14&z=3&v=-54.13349998138993,66.35888052399868,-50.32103113049877,69.08420005412792), where a clear smoke signal was recorded. A CALIOP overpass through the edge of the plume allows studying its vertical structure. Increased attenuated backscatter is found below ~1.5 km above sea level between 52°E and 51°E (Figure 6b; black line denotes the orography). Figure 6c (red line), shows that the CALIOP overpass transects directly the simulated plume of the Greenland fires. Notice that the simulated plume also agrees very well with the smoke as seen in NASA's ESDIS picture (Figure 6a). The vertical distribution of simulated BC as a function of longitude is illustrated in Figure 6d. It corresponds very well to the vertical distribution of aerosols observed by CALIOP (Figure 6b). In particular, the smoke resides at altitudes below 1.5 km and at exactly the same location both in the simulations and observations.

4.2 Radiative forcing and albedo effects

BOA IRF for noon on 31 August 2017 is depicted in Figure 7, both for cloudless (Fig. 7a) and cloudy conditions (Fig. 7b). This day is shown because almost all BC emitted by the fires had been deposited before, thus giving a high IRF via albedo reduction due to BC contamination of snow. For the cloudless conditions, the IRF is largest over ice close to the fire site and at locations with relatively large BC deposits. The maximum IRF is 1.82 W m^{-2}, while the average for Greenland is 0.05 W m^{-2}. For the IRF including clouds the maximum BOA (TOA) RF is 0.63 W m^{-2} (0.59 W m^{-2}), and the average 0.03 W m^{-2} (0.03 W m^{-2}).

Clouds are thus found to reduce the maximum BOA IRF by a factor of 2.9 and the average BOA IRF by a factor of 1.7.

The IRF depends on the optical properties of the smoke from the fire, which are not known. Hence, a sensitivity analysis was performed where the single scattering albedo (SSA) was perturbed in contrast to a "medium case" (Figure S 7a) that was adopted from the SNICAR model (Flanner et al., 2007, 2009) and has been used for the discussion in the previous paragraph. To estimate the uncertainty due to the choice of BC optical properties, additional calculations were made by scaling the SSA (red solid lines in Figure S 7a). The choices of these scaled SSA values were based on the SSA reported for various modified combustion efficiencies (MCE) by Pokhrel et al. (2016). Pokhrel et al. (2016) reported an MCE of 0.9 for peat land. As such, our adopted SSA may be considered low (compare black solid line and red line with upward triangles). Figure S 7b shows the IRF as BC is deposited for the three cases. It suggests that the IRF ranges between 40% and 130% of our above assumed medium-case values for realistic variation of the aerosol optical properties.

Figure 7d depicts the temporal behaviour of the cloudy TOA IRF averaged over Greenland (red line). In addition the daily averaged IRF is shown (green line). The daily averaged IRF is seen to increase as the plume from the fires spreads out and starts to decline after the fires were extinguished at the end of the month. The fact that the reduction towards end of August is relatively slow is caused by the effect of the albedo reduction, which persists until clean snow covers the polluted snow. Overall, albedo reduction dominates the total IRF averaged over Greenland for the period of study contributing between 85% (in the beginning of the study period) to 99% (at the end of the study period) and increasing in relative importance with time as atmospheric BC is removed.

According to Hansen et al. (2005) the TOA IRF of BC approximates the adjusted RF as reported by Myhre et al. (2013). In their Table 8.4, Myhre et al. (2013) estimated the global averaged RF due to BC between the years 1750 and 2011 to be +0.40 (+0.05 to +0.80) W m^{-2}. Skeie et al. (2011) estimated a global mean radiative forcing of 0.35 W m^{-2} due to fossil fuel and biofuel increases between 1750 and 2000. For Greenland, Skeie et al. (2011) found the RF to be less than about 0.2 W m^{-2}. This number may be compared to our area averaged IRF estimate due to the Greenland fire. For cloudy conditions the TOA IRF over Greenland due to the Greenland fires is about one order of magnitude smaller compared with the RF over Greenland due to BC from all global anthropogenic sources reported in Skeie et al. (2011).

The albedo reduction at 550 nm due to the deposited BC from the Greenland fires is shown in Figure 7c. The maximum albedo change is about 0.006. This albedo change has an impact on IRF, but it is too small to be measured by satellites. For example, MODIS albedo estimates have been compared to in situ albedo measurements in Greenland by Stroeve et al. (2005). They found that the root mean square error between MODIS and in situ albedo values was ±0.04 for high quality flagged MODIS albedo retrievals. Unmanned Aerial Vehicle (UAV) measurements over Greenland made by Burkhart et al. (2017) have uncertainties of similar magnitude. Also, Polashenski et al. (2015) reported that the albedo reduction due to aerosol impurities on the Greenland Ice Sheet in 2012–2014 period is relatively small (mean 0.003), though episodic aerosol deposition events can reduce albedo by 0.01–0.02. The albedo changes due to BC from the Greenland fires are generally an order of magnitude smaller (Figure 7c) and thus too small to be detected by present UAV and satellite instruments and retrieval methods (Warren, 2013).

5 Conclusions

The conclusions from our study of the unusual open fires burning in Greenland between 31 July and 21 August 2017 are the following:

- The fires burned on peat lands that became vulnerable by permafrost thawing. The region where the fires burned was identified previously as being susceptible to permafrost melting; however, large-scale melting was expected to occur only towards the end of the 21st century. The 2017 fires show that at least in some locations substantial permafrost thawing is occurring already now.
- The total area burned was about 2345 hectares. We estimate that the fires consumed a fuel amount of about 117 kt C and produced BC emissions of about 23.5 t.
- The Greenland fires were small compared to fires burning at the same time in North America and Eurasia, but a large fraction of their BC emissions (30% or 7 t) was deposited on the Greenland Ice Sheet or glaciers.
- Measurements of aerosol optical depth at three sites in Western Greenland in August 2017 were strongly influenced by forest fires in Canada burning at the same time, but the Greenland fires had an observable impact doubling the column-integrated BC concentrations only at the closest station.
- A comparison of the simulated BC releases in FLEXPART with the vertical cross-section of total attenuated backscatter (at 532 nm) from CALIOP lidar showed that the spatiotemporal evolution and particularly the top height of the plume was captured by the model.

- We estimate that the maximum albedo change due to the BC deposition from the Greenland fires was about 0.006, too small to be measured by satellites or other means. The average instantaneous BOA radiative forcing over Greenland at noon on 31 August was 0.03 W m^{-2}, with locally occurring maximum values of 0.63 W m^{-2}. The average value is at least an order of magnitude smaller than the radiative forcing due to BC from other sources.
- We conclude that the fires burning in Greenland in summer of 2017 had little impact on BC deposition on the Greenland Ice Sheet, causing almost negligible extra radiative forcing. This was due to the – in a global context - still rather small size of the fires.

The very large fraction of the BC emissions deposited on the Greenland Ice Sheet (30% of the emissions) makes these fires very efficient climate forcers on a per unit emission basis. Thus, while the fires in 2017 were still relatively small on a global scale, if the expected future warming of the Arctic (IPCC, 2013) produces more and larger fires in Greenland in the future (Keegan et al., 2014), this could indeed cause substantial albedo changes and thus contribute to accelerated melting of the Greenland Ice Sheet.

Data availability. All data used for the present publication can be obtained from the corresponding author upon request.

Competing financial interests. The authors declare no competing financial interests.

Acknowledgements. This study was partly supported by the Arctic Monitoring and Assessment Programme (AMAP) and was conducted as part of the Nordic Centre of Excellence eSTICC (Nordforsk 57001). We acknowledge the use of imagery from the NASA Worldview application (https://worldview.earthdata.nasa.gov/) operated by the NASA/Goddard Space Flight Center Earth Science Data and Information System (ESDIS) project. We thank Brent Holben and local site managers for their effort in establishing and maintaining the AERONET sites used in this investigation. We thank NASA/CNES engineers and scientists for making CALIOP data available. The lidar data were downloaded from the ICARE Data and Service Center.

Author contributions. NE performed the simulations, analyses, wrote and coordinated the paper. AK performed the radiation calculations and wrote parts of the paper. VM and SZ performed GIS analysis for the burned area calculations. RP made all the runs for the injection height calculations using the PRMv2 model. KS analysed satellite data for AOD and CALIOP, SE and AS commented and coordinated the manuscript. All authors contributed to the final version of the manuscript.

References

Abdalati, W. and Steffen, K.: Greenland Ice Sheet melt extent:1979-1999, J. Geophys. Res. Atmos., 106(D24), 33983–33988, doi:10.1029/2001JD900181, 2001.

Akagi, S. K., Yokelson, R. J., Wiedinmyer, C., Alvarado, M. J., Reid, J. S., Karl, T., Crounse, J. D. and Wennberg, P. O.: Emission factors for open and domestic biomass burning for use in atmospheric models, Atmos. Chem. Phys., 11(9), 4039–4072, doi:10.5194/acp-11-4039-2011, 2011.

AMAP: Snow, Water, Ice and Permafrost. Summary for Policy-makers, Arctic Monitoring and Assessment Programme (AMAP), Oslo, Norway. [online] Available from: https://www.amap.no/documents/doc/Snow-Water-Ice-and-Permafrost.-Summary-for-Policy-makers/1532 (Accessed 27 November 2017), 2017.

BBC News: "Unusual" Greenland wildfires linked to peat, [online] Available from: http://www.bbc.com/news/science-environment-40877099 (Accessed 6 September 2017), 2017.

Bellouin, N. and Haywood, J.: Aerosols: Climatology of Tropospheric Aerosols, Second Edi., Elsevier., 2014.

Benscoter, B. W. and Wieder, R. K.: Variability in organic matter lost by combustion in a boreal bog during the 2001 Chisholm fire, Can. J. For. Res., 33(12), 2509–2513, doi:10.1139/x03-162, 2003.

Bond, T. C., Doherty, S. J., Fahey, D. W., Forster, P. M., Berntsen, T., Deangelo, B. J., Flanner, M. G., Ghan, S., Kärcher, B., Koch, D., Kinne, S., Kondo, Y., Quinn, P. K., Sarofim, M. C., Schultz, M. G., Schulz, M., Venkataraman, C., Zhang, H., Zhang, S., Bellouin, N., Guttikunda, S. K., Hopke, P. K., Jacobson, M. Z., Kaiser, J. W., Klimont, Z., Lohmann, U., Schwarz, J. P., Shindell, D., Storelvmo, T., Warren, S. G. and Zender, C. S.: Bounding the role of black carbon in the climate system: A scientific assessment, J. Geophys. Res. Atmos., 118(11), 5380–5552, doi:10.1002/jgrd.50171, 2013.

Buras, R., Dowling, T. and Emde, C.: New secondary-scattering correction in DISORT with increased efficiency for forward scattering, J. Quant. Spectrosc. Radiat. Transf., 112(12), 2028–2034, doi:10.1016/j.jqsrt.2011.03.019, 2011.

Chavez, P. S.: An improved dark-object subtraction technique for atmospheric scattering correction of multispectral data, Remote Sens. Environ., 24(3), 459–479, doi:10.1016/0034-4257(88)90019-3, 1988.

Cofer III, W. R., Levine, J. S., Winstead, E. L. and Stocks, B. J.: New estimates of nitrous oxide emissions from biomass burning, Nature, 349(6311), 689–691 [online] Available from: http://dx.doi.org/10.1038/349689a0, 1991.

Conny, J. and Slater, J.: Black carbon and organic carbon in aerosol particles from crown fires in the Canadian boreal forest, J. Geophys. Res. … [online] Available from: http://onlinelibrary.wiley.com/doi/10.1029/2001JD001528/full, 2002.

Daanen, R. P., Ingeman-Nielsen, T., Marchenko, S. S., Romanovsky, V. E., Foged, N., Stendel, M., Christensen, J. H. and Hornbech Svendsen, K.: Permafrost degradation risk zone assessment using simulation models, Cryosphere, 5(4), 1043–1056, doi:10.5194/tc-5-1043-2011, 2011.

Dahlback, A. and Stamnes, K.: A new spherical model for computing the radiation field available for photolysis and heating at twilight, Planet. Space Sci., 39(5), 671–683, doi:10.1016/0032-0633(91)90061-E, 1991.

Davies, G. M., Gray, A., Rein, G. and Legg, C. J.: Peat consumption and carbon loss due to smouldering wildfire in a temperate peatland, For. Ecol. Manage., 308, 169–177, doi:10.1016/j.foreco.2013.07.051, 2013.

Doherty, S. J., Warren, S. G., Grenfell, T. C., Clarke, A. D. and Brandt, R. E.: Light-absorbing impurities in Arctic snow, Atmos. Chem. Phys., 10(23), 11647–11680, doi:10.5194/acp-10-11647-2010, 2010.

Drysdale, D.: An Introduction to Fire Dynamics, 3rd Editio., John Wiley & Sons, Ltd., 2011.

Emde, C., Buras-Schnell, R., Kylling, A., Mayer, B., Gasteiger, J., Hamann, U., Kylling, J., Richter, B., Pause, C., Dowling, T. and Bugliaro, L.: The libRadtran software package for radiative transfer calculations (version 2.0.1), Geosci. Model Dev., 9(5), 1647–1672, doi:10.5194/gmd-9-1647-2016, 2016.

Escuin, S., Navarro, R. and Fernández, P.: Fire severity assessment by using NBR (Normalized Burn Ratio) and NDVI (Normalized Difference Vegetation Index) derived from LANDSAT TM/ETM images, Int. J. Remote Sens., 29(4), 1053–1073, doi:10.1080/01431160701281072, 2008.

Evangeliou, N., Balkanski, Y., Cozic, A., Hao, W. M. and Møller, A. P.: Wildfires in Chernobyl-contaminated forests and risks to the population and the environment: A new nuclear disaster about to happen?, Environ. Int., 73, 346–358, doi:10.1016/j.envint.2014.08.012, 2014.

Evangeliou, N., Balkanski, Y., Cozic, A., Hao, W. M., Mouillot, F., Thonicke, K., Paugam, R., Zibtsev, S., Mousseau, T. A., Wang, R., Poulter, B., Petkov, A., Yue, C., Cadule, P., Koffi, B., Kaiser, J. W., Møller, A. P. and Classen, A. T.: Fire evolution in the radioactive forests of Ukraine and Belarus: Future risks for the population and the environment, Ecol. Monogr., 85(1), 49–72, doi:10.1890/14-1227.1, 2015.

Evangeliou, N., Zibtsev, S., Myroniuk, V., Zhurba, M., Hamburger, T., Stohl, A., Balkanski, Y., Paugam, R., Mousseau, T. A., Møller, A. P. and Kireev, S. I.: Resuspension and atmospheric transport of radionuclides due to wildfires near the Chernobyl Nuclear Power Plant in 2015: An impact assessment., Sci. Rep., 6, 26062 [online] Available from: http://www.nature.com/srep/2016/160517/srep26062/full/srep26062.html, 2016.

Fang, X., Thompson, R. L., Saito, T., Yokouchi, Y., Kim, J., Li, S., Kim, K. R., Park, S., Graziosi, F. and Stohl, A.: Sulfur hexafluoride (SF6) emissions in East Asia determined by inverse modeling, Atmos. Chem. Phys., 14(9), 4779–4791, doi:10.5194/acp-14-4779-2014, 2014.

Faulkner Burkhart, J., Kylling, A., Schaaf, C. B., Wang, Z., Bogren, W., Storvold, R., Solbø, S., Pedersen, C. A. and Gerland, S.: Unmanned aerial system nadir reflectance and MODIS nadir BRDF-adjusted surface reflectances intercompared over Greenland, Cryosphere, 11(4), 1575–1589, doi:10.5194/tc-11-1575-2017, 2017.

Ferguson, S. A., Collins, R. L., Ruthford, J. and Fukuda, M.: Vertical distribution of nighttime smoke following a wildland biomass fire in boreal Alaska, J. Geophys. Res., 108(June), D23, 4743, doi:10.1029/2002JD003324, doi:10.1029/2002JD003324, 2003.

Fernandez Anez, N., Garcia Torrent, J., Medic Pejic, L. and Grima Olmedo, C.: Detection of incipient self-ignition process in solid fuels through gas emissions methodology, J. Loss Prev. Process Ind., 36, 343–351, doi:10.1016/j.jlp.2015.02.010, 2015.

Flanner, M. G., Zender, C. S., Randerson, J. T. and Rasch, P. J.: Present-day climate forcing and response from black carbon in snow, J. Geophys. Res. Atmos., 112(11), 1–17, doi:10.1029/2006JD008003, 2007.

Flanner, M. G., Zender, C. S., Hess, P. G., Mahowald, N. M., Painter, T. H., Ramanathan, V. and Rasch, P. J.: Springtime warming and reduced snow cover from carbonaceous particles, Atmos. Chem. Phys., 9, 2481–2497, doi:10.5194/acp-9-2481-2009, 2009.

Forster, C., Wandinger, U., Wotawa, G., James, P., Mattis, I., Althausen, D., Simmonds, P., O'Doherty, S., Jennings, S. G., Kleefeld, C., Schneider, J., Trickl, T., Kreipl, S., Jäger, H. and Stohl, A.: Transport of boreal forest fire emissions from Canada to Europe, J. Geophys. Res., 106, 22887, doi:10.1029/2001JD900115, 2001.

Forster, C., Stohl, A. and Seibert, P.: Parameterization of convective transport in a Lagrangian particle dispersion model and its evaluation, J. Appl. Meteorol. Climatol., 46(4), 403–422, doi:10.1175/JAM2470.1, 2007.

Freitas, S. R., Longo, K. M., Chatfield, R., Latham, D., Silva Dias, M. a. F., Andreae, M. O., Prins, E., Santos, J. C., Gielow, R. and Carvalho, J. a.: Including the sub-grid scale plume rise of vegetation fires in low resolution atmospheric transport models, Atmos. Chem. Phys. Discuss., 6(6), 11521–11559, doi:10.5194/acpd-6-11521-2006, 2006.

Freitas, S. R., Longo, K. M., Trentmann, J. and Latham, D.: Technical Note: Sensitivity of 1-D smoke plume rise models to the inclusion of environmental wind drag, Atmos. Chem. Phys., 10(2), 585–594, doi:10.5194/acp-10-585-2010, 2010.

French, N., Kasischke, E., Hall, R., Murphy, K., Verbyla, D., Hoy, E. and Allen, J.: Using Landsat data to assess fire and burn severity in the North American boreal forest region: an overview and summary of results, Int. J. Wildl. Fire, 17(4), 443–462, doi:10.1071/WF08007, 2008.

Fromm, M., Bevilacqua, R., Servranckx, R., Rosen, J., Thayer, J. P., Herman, J. and Larko, D.: Pyro-cumulonimbus injection of smoke to the stratosphere: Observations and impact of a super blowup in northwestern Canada on 3-4 August 1998, J. Geophys. Res. D Atmos., 110(8), 1–17, doi:10.1029/2004JD005350, 2005.

Giglio, L., Descloitres, J., Justice, C. O. and Kaufman, Y. J.: An enhanced contextual fire detection algorithm for MODIS, Remote Sens. Environ., 87(2–3), 273–282, doi:10.1016/S0034-4257(03)00184-6, 2003.

Grythe, H., Kristiansen, N. I., Groot Zwaaftink, C. D., Eckhardt, S., Ström, J., Tunved, P., Krejci, R. and Stohl, A.: A new aerosol wet removal scheme for the Lagrangian particle model FLEXPARTv10, Geosci. Model Dev., 10, 1447–1466, doi:10.5194/gmd-10-1447-2017, 2017.

Hansen, J. and Nazarenko, L.: Soot climate forcing via snow and ice albedos, Proc. Natl. Acad. Sci. U. S. A., 101(2), 423–428, doi:10.1073/pnas.2237157100, 2004.

Hansen, J., Sato, M., Ruedy, R., Nazarenko, L., Lacis, A., Schmidt, G. A., Russell, G., Aleinov, I., Bauer, M., Bauer, S., Bell, N., Cairns, B., Canuto, V., Chandler, M., Cheng, Y., Del Genio, A., Faluvegi, G., Fleming, E., Friend, A., Hall, T., Jackman, C., Kelley, M., Kiang, N., Koch, D., Lean, J., Lerner, J., Lo, K., Menon, S., Miller, R., Minnis, P., Novakov, T., Oinas, V., Perlwitz, J., Perlwitz, J., Rind, D., Romanou, A., Shindell, D., Stone, P., Sun, S., Tausnev, N., Thresher, D., Wielicki, B., Wong, T., Yao, M. and Zhang, S.: Efficacy of climate forcings, J. Geophys. Res. D Atmos., 110(18), 1–45, doi:10.1029/2005JD005776, 2005.

Hao, W. M. and Ward, D. E.: Methane production from global biomass burning, J. Geophys. Res. Atmos., 98(D11), 20657–20661, doi:10.1029/93JD01908, 1993.

Hao, W. M., Petkov, A., Nordgren, B. L., Silverstein, R. P., Corley, R. E., Urbanski, S. P., Evangeliou, N., Balkanski, Y. and Kinder, B.: Daily black carbon emissions from fires in Northern Eurasia from 2002 to 2013, Geosci. Model Dev., 9, 4461–4474, doi:10.5194/gmd-9-4461-2016, 2016.

Holben, B. N.: Characteristics of maximum-value composite images from temporal AVHRR data, Int. J. Remote Sens., 7(11), 1417–1434, doi:10.1080/01431168608948945, 1986.

Holben, B. N., Eck, T. F., Slutsker, I., Tanré, D., Buis, J. P., Setzer, A., Vermote, E., Reagan, J. A., Kaufman, Y. J., Nakajima, T., Lavenu, F., Jankowiak, I. and Smirnov, A.: AERONET—A Federated Instrument Network and Data Archive for Aerosol Characterization, Remote Sens. Environ., 66(1), 1–16, doi:10.1016/S0034-4257(98)00031-5, 1998.

Hosseini, S., Li, Q., Cocker, D., Weise, D., Miller, A., Shrivastava, M., Miller, J. W., Mahalingam, S., Princevac, M. and Jung, H.: Particle size distributions from laboratory-scale biomass fires using fast response instruments, Atmos. Chem. Phys., 10(16), 8065–8076, doi:10.5194/acp-10-8065-2010, 2010.

IPCC: Climate Change 2013: The Physical Science Basis. Contribution to the Fifth Assessment Report of the Intergovernmental Panel on Climate Change., edited by T. F. Stocker, D. Qin, G.-K. Plattner, M. M. B. Tignor, S. K. Allen, J. Boschung, A. Nauels, Y. Xia, V. Bex, and P. M. Midgley, Cambridge University Press., 2013.

Jedrzejek, B., Drees, B., Daniëls, F. J. A. and Hölzel, N.: Vegetation pattern of mountains in West Greenland - a baseline for long-term surveillance of global warming impacts, Plant Ecol. Divers., 6(3–4), 405–422, doi:10.1080/17550874.2013.802049, 2013.

Justice, C. O., Giglio, L., Korontzi, S., Owens, J., Morisette, J. T., Roy, D., Descloitres, J., Alleaume, S., Petitcolin, F. and Kaufman, Y.: The MODIS fire products, Remote Sens. Environ., 83(1–2), 244–262, doi:10.1016/S0034-4257(02)00076-7, 2002.

Kaiser, J. W., Heil, A., Andreae, M. O., Benedetti, A., Chubarova, N., Jones, L., Morcrette, J. J., Razinger, M., Schultz, M. G., Suttie, M. and Van Der Werf, G. R.: Biomass burning emissions estimated with a global fire assimilation system based on observed fire radiative power, Biogeosciences, 9(1), 527–554, doi:10.5194/bg-9-527-2012, 2012.

Kato, S., Ackerman, T. P., Mather, J. H. and Clothiaux, E. E.: The k-distribution method and correlated-k approximation for a shortwave radiative transfer model, J. Quant. Spectrosc. Radiat. Transf., 62(1), 109–121, doi:10.1016/S0022-4073(98)00075-2, 1999.

Keegan, K. M., Albert, M. R., Mcconnell, J. R. and Baker, I.: Climate change and forest fires synergistically drive widespread melt events of the Greenland Ice Sheet, , 1–4, doi:10.1073/pnas.1405397111, 2014.

Key, C. H. and Benson, N. C.: Landscape assessment: Sampling and analysis methods, USDA For. Serv. Gen. Tech. Rep. RMRS-GTR-164-CD, (June), 1–55, doi:10.1002/app.1994.070541203, 2006.

Klimont, Z., Kupiainen, K., Heyes, C., Purohit, P., Cofala, J., Rafaj, P., Borken-Kleefeld, J. and Schöpp, W.: Global anthropogenic emissions of particulate matter including black carbon, Atmos. Chem. Phys., 17, 8681–8723, doi:10.5194/acp-17- 50 8681-2017, 2017.

Lavoie, C. and Pellerin, S.: Fires in temperate peatlands (southern Quebec): past and recent trends, Can. J. Bot., 85(3), 263–272, doi:10.1139/B07-012, 2007.

Legrand, M., McConnell, J., Fischer, H., Wolff, E. W., Preunkert, S., Arienzo, M., Chellman, N., Leuenberger, D., Maselli, O., Place, P., Sigl, M., Schï¿½pbach, S. and Flannigan, M.: Boreal fire records in Northern Hemisphere ice cores: A review, Clim. Past, 12(10), 2033–2059, doi:10.5194/cp-12-2033-2016, 2016.

Leino, K., Riuttanen, L., Nieminen, T., Väänänen, R., Pohja, T., Keronen, P., Järvi, L., Aalto, P. P., Virkkula, A., Kerminen, V. M., Petäjä, T., Kulmala, M., Nieminen, T., Dal Maso, M. and Virkkula, A.: Biomass-burning smoke episodes in Finland from eastern European wildfires, Boreal Environ. Res., 19(x), 275–292, 2014.

Lelieveld, J., Evans, J. S., Fnais, M., Giannadaki, D. and Pozzer, A.: The contribution of outdoor air pollution sources to premature mortality on a global scale., Nature, 525(7569), 367–71, doi:10.1038/nature15371, 2015.

Leung, F. Y. T., Logan, J. A., Park, R., Hyer, E., Kasischke, E., Streets, D. and Yurganov, L.:

Impacts of enhanced biomass burning in the boreal forests in 1998 on tropospheric chemistry and the sensitivity of model results to the injection height of emissions, J. Geophys. Res. Atmos., 112(10), 1–15, doi:10.1029/2006JD008132, 2007.

Long, C. M., Nascarella, M. A. and Valberg, P. A.: Carbon black vs. black carbon and other airborne materials containing elemental carbon: Physical and chemical distinctions, Environ. Pollut., 181, 271–286, doi:10.1016/j.envpol.2013.06.009, 2013.

Magnan, G., Lavoie, M. and Payette, S.: Impact of fire on long-term vegetation dynamics of ombrotrophic peatlands in northwestern Québec, Canada, Quat. Res., 77(1), 110–121, doi:http://dx.doi.org/10.1016/j.yqres.2011.10.006, 2012.

Massling, A., Nielsen, I. E., Kristensen, D., Christensen, J. H., Sorensen, L. L., Jensen, B., Nguyen, Q. T., Nøjgaard, J. K., Glasius, M. and Skov, H.: Atmospheric black carbon and sulfate concentrations in Northeast Greenland, Atmos. Chem. Phys., 15(16), 9681–9692, doi:10.5194/acp-15-9681-2015, 2015.

Mayer, B. and Kylling, A.: Technical note: The libRadtran software package for radiative transfer calculations - description and examples of use, Atmos. Chem. Phys., 5(7), 1855–1877, doi:10.5194/acp-5-1855-2005, 2005.

Myhre, G., Shindell, D., Bréon, F.-M., Collins, W., Fuglestvedt, J., Huang, J., Koch, D., Lamarque, J.-F., Lee, D., Mendoza, B., Nakajima, T., Robock, A., Stephens, G., Takemura, T. and Zhang, H.: Anthropogenic and Natural Radiative Forcing, in Climate Change 2013: The Physical Science Basis. Contribution of Working Group I to the Fifth Assessment Report of the Intergovernmental Panel on Climate Change, edited by Stocker, T.F., D. Qin, G.-K. Plattner, M. Tignor, S. K. Allen, J. Boschung, A. Nauels, Y. Xia, V. Bex, and P. M. Midgley, pp. 659–740, Cambridge University Press, Cambridge, United Kingdom and New York, NY, USA., 2013.

NASA: FIRMS. Web Fire Mapper, [online] Available from: https://firms.modaps.eosdis.nasa.gov/firemap/ (Accessed 5 September 2017a), 2017.

NASA: Roundtable: The Greenland Wildfire, [online] Available from: https://earthobservatory.nasa.gov/blogs/earthmatters/2017/08/10/roundtable-the-greenland-wildfire/ (Accessed 6 September 2017b), 2017.

NASA: Wildfires Continue to Beleaguer Western Canada, [online] Available from: https://www.nasa.gov/image-feature/goddard/2017/wildfires-continue-to-beleaguer-western-canada (Accessed 29 October 2017c), 2017.

New Scientist Magazine: Largest ever wildfire in Greenland seen burning from space, [online] Available from: https://www.newscientist.com/article/2143159-largest-ever-wildfire-in-greenland-seen-burning-from-space/ (Accessed 6 September 2017), 2017.

Page, S. E., Siegert, F., Rieley, J. O., Boehm, H.-D. V., Jada, A. and Limin, S.: The amount of carbon released from peat and forest fires in Indonesia during 1997, Nature, 420(19), 61–65, doi:10.1038/nature01131, 2015.

Paugam, R., Wooster, M. and Atherton, J.: Development and optimization of a wildfire plume rise model based on remote sensing data inputs – Part 2, , doi:10.5194/acpd-15-9815-2015, 2015.

Pokhrel, R. P., Wagner, N. L., Langridge, J. M., Lack, D. A., Jayarathne, T., Stone, E. A., Stockwell, C. E., Yokelson, R. J. and Murphy, S. M.: Parameterization of single-scattering albedo (SSA) and absorption Ångström exponent (AAE) with EC/OC for aerosol emissions from biomass burning, Atmos. Chem. Phys., 16(15), 9549–9561, doi:10.5194/acp-16-9549-2016, 2016.

Polashenski, C. M., Dibb, J. E., Flanner, M. G., Chen, J. Y., Courville, Z. R., Lai, A. M., Schauer, J. J., Shafer, M. M. and Bergin, M.: Neither dust nor black carbon causing apparent albedo decline in Greenland's dry snow zone: Implications for MODIS C5 surface reflectance, Geophys. Res. Lett., 42(21), 9319–9327, doi:10.1002/2015GL065912, 2015.

Randerson, J. T., Chen, Y., Van Der Werf, G. R., Rogers, B. M. and Morton, D. C.: Global burned area and biomass burning emissions from small fires, J. Geophys. Res. Biogeosciences, 117(4), doi:10.1029/2012JG002128, 2012.

Reddy, A. D., Hawbaker, T. J., Wurster, F., Zhu, Z., Ward, S., Newcomb, D. and Murray, R.: Quantifying soil carbon loss and uncertainty from a peatland wildfire using multi-temporal LiDAR, Remote Sens. Environ., 170, 306–316, doi:10.1016/j.rse.2015.09.017, 2015.

Rémy, S., Veira, A., Paugam, R., Sofiev, M., Kaiser, J. W., Marenco, F., Burton, S. P., Benedetti, A., Engelen, R. J., Ferrare, R. and Hair, J. W.: Two global data sets of daily fire emission injection heights since 2003, , 2921–2942, doi:10.5194/acp-17-2921-2017, 2017.

Restuccia, F., Ptak, N. and Rein, G.: Self-heating behavior and ignition of shale rock, Combust. Flame, 176, 213–219, doi:10.1016/j.combustflame.2016.09.025, 2017a.

Restuccia, F., Huang, X. and Rein, G.: Self-ignition of natural fuels: Can wildfires of carbon-rich soil start by self-heating?, Fire Saf. J., 91(February), 828–834, doi:10.1016/j.firesaf.2017.03.052, 2017b.

Sand, M., Berntsen, T. K., von Salzen, K., Flanner, M. G., Langner, J. and Victor, D. G.: Response of Arctic temperature to changes in emissions of short-lived climate forcers, Nat. Clim. Chang., 6(November), 1–5, doi:10.1038/nclimate2880, 2015.

von Schneidemesser, E., Schauer, J. J., Hagler, G. S. W. and Bergin, M. H.: Concentrations and sources of carbonaceous aerosol in the atmosphere of Summit, Greenland, Atmos. Environ., 43(27), 4155–4162, doi:10.1016/j.atmosenv.2009.05.043, 2009.

Seiler, W. and Crutzen, P. J.: Estimates of gross and net fluxes of carbon between the biosphere and the atmosphere from biomass burning, Clim. Change, 2(3), 207–247, doi:10.1007/BF00137988, 1980.

SERMITSIAQ: Se billeder: Naturbrand udvikler kraftig røg, , in Danish [online] Available from: http://sermitsiaq.ag/se-billeder-naturbrand-udvikler-kraftig-roeg (Accessed 6 September 2017), 2017.

Shetler, G., Turetsky, M. R., Kane, E. and Kasischke, E.: Sphagnum mosses limit total carbon consumption during fire in Alaskan black spruce forests, Can. J. For. Res., 38(8), 2328–2336, doi:10.1139/X08-057, 2008.

Shi, Y., Matsunaga, T., Saito, M., Yamaguchi, Y. and Chen, X.: Comparison of global inventories of CO2 emissions from biomass burning during 2002-2011 derived from multiple satellite products, Environ. Pollut., 206, 479–487, doi:10.1016/j.envpol.2015.08.009, 2015.

Skeie, R. B., Berntsen, T., Myhre, G., Pedersen, C. A., Strãm, J., Gerland, S. and Ogren, J. A.: Black carbon in the atmosphere and snow, from pre-industrial times until present, Atmos. Chem. Phys., 11(14), 6809–6836, doi:10.5194/acp-11-6809-2011, 2011.

Smirnov, N. S., Korotkov, V. N. and Romanovskaya, A. A.: Black carbon emissions from wildfires on forest lands of the Russian Federation in 2007–2012, Russ. Meteorol. Hydrol., 40(7), 435–442, doi:10.3103/S1068373915070018, 2015.

Stamnes, K., Tsay, S.-C., Wiscombe, W. and Jayaweera, K.: Numerically stable algorithm for discrete-ordinate-method radiative transfer in multiple scattering and emitting layered media, Appl. Opt., 27(12), 2502, doi:10.1364/AO.27.002502, 1988.

Stendel, M., Christensen, J. H. and Petersen, D.: Arctic Climate and Climate Change with a Focus on Greenland, Adv. Ecol. Res., 40(07), 13–43, doi:10.1016/S0065-2504(07)00002-5, 2008.

Stockwell, C. E., Jayarathne, T., Cochrane, M. A., Ryan, K. C., Putra, E. I., Saharjo, B. H., Nurhayati, A. D., Albar, I., Blake, D. R., Simpson, I. J., Stone, E. A. and Yokelson, R. J.: Field measurements of trace gases and aerosols emitted by peat fires in Central Kalimantan, Indonesia, during the 2015 El Niño, Atmos. Chem. Phys., 16(18), 11711–11732, doi:10.5194/acp-16-11711-2016, 2016.

Stohl, A., Forster, C., Frank, A., Seibert, P. and Wotawa, G.: Technical note: The Lagrangian particle dispersion model FLEXPART version 6.2, Atmos. Chem. Phys., 5(9), 2461–2474, doi:10.5194/acp-5-2461-2005, 2005.

Stohl, A., Andrews, E., Burkhart, J. F., Forster, C., Herber, A., Hoch, S. W., Kowal, D., Lunder, C., Mefford, T., Ogren, J. A., Sharma, S., Spichtinger, N., Stebel, K., Stone, R., Ström, J., Tørseth, K., Wehrli, C. and Yttri, K. E.: Pan-Arctic enhancements of light absorbing aerosol concentrations due to North American boreal forest fires during summer 2004, J. Geophys. Res. Atmos., 111(22), 1–20, doi:10.1029/2006JD007216, 2006.

Stohl, A., Berg, T., Burkhart, J. F., Fjǽraa, A. M., Forster, C., Herber, A., Hov, Ø., Lunder, C., McMillan, W. W., Oltmans, S., Shiobara, M., Simpson, D., Solberg, S., Stebel, K., Ström, J., Tørseth, K., Treffeisen, R., Virkkunen, K. and Yttri, K. E.: Arctic smoke – record high air pollution levels in the European Arctic due to agricultural fires in Eastern Europe in spring 2006, Atmos. Chem. Phys., 7(2), 511–534, doi:10.5194/acp-7-511-2007, 2007.

Stohl, A., Prata, A. J., Eckhardt, S., Clarisse, L., Durant, A., Henne, S., Kristiansen, N. I., Minikin, A., Schumann, U., Seibert, P., Stebel, K., Thomas, H. E., Thorsteinsson, T., Tørseth, K. and Weinzierl, B.: Determination of time-and height-resolved volcanic ash emissions and their use for quantitative ash dispersion modeling: The 2010 Eyjafjallajokull eruption, Atmos. Chem. Phys., 11(9), 4333–4351, doi:10.5194/acp-11-4333-2011, 2011.

Stohl, A., Klimont, Z., Eckhardt, S., Kupiainen, K., Shevchenko, V. P., Kopeikin, V. M. and Novigatsky, A. N.: Black carbon in the Arctic: The underestimated role of gas flaring and residential combustion emissions, Atmos. Chem. Phys., 13(17), 8833–8855, doi:10.5194/acp-13-8833-2013, 2013.

Stroeve, J., Box, J. E., Gao, F., Liang, S., Nolin, A. and Schaaf, C.: Accuracy assessment of the MODIS 16-day albedo product for snow: Comparisons with Greenland in situ measurements, Remote Sens. Environ., 94(1), 46–60, doi:10.1016/j.rse.2004.09.001, 2005.

Sunderman, S. O. and Weisberg, P. J.: Remote sensing approaches for reconstructing fire perimeters and burn severity mosaics in desert spring ecosystems, Remote Sens. Environ., 115(9), 2384–2389, doi:10.1016/j.rse.2011.05.001, 2011.

Turetsky, M. R., Donahue, W. F. and Benscoter, B. W.: Experimental drying intensifies burning and carbon losses in a northern peatland, Nat. Commun., 2, 514, doi:10.1038/ncomms1523, 2011.

Turetsky, M. R., Benscoter, B., Page, S., Rein, G., van der Werf, G. R. and Watts, A.: Global vulnerability of peatlands to fire and carbon loss, Nat. Geosci., 8(1), 11–14, doi:10.1038/ngeo2325, 2014.

Urbanski, S. P., Hao, W. M. and Nordgren, B.: The wildland fire emission inventory: Western United States emission estimates and an evaluation of uncertainty, Atmos. Chem. Phys., 11(24), 12973–13000, doi:10.5194/acp-11-12973-2011, 2011.

Wandji Nyamsi, W., Arola, A., Blanc, P., Lindfors, a. V., Cesnulyte, V., Pitkänen, M. R. a. and Wald, L.: Technical Note: A novel parameterization of the transmissivity due to ozone absorption in the distribution method and correlated approximation of Kato et al. (1999) over the UV band, Atmos. Chem. Phys., 15(13), 7449–7456, doi:10.5194/acp-15-7449-2015, 2015.

Warren, S. G.: Can black carbon in snow be detected by remote sensing?, J. Geophys. Res.

Atmos., 118(2), 779–786, doi:10.1029/2012JD018476, 2013.

Wieder, R. K., Scott, K. D., Kamminga, K., Vile, M. A., Vitt, D. H., Bone, T., Xu, B., Benscoter, B. W. and Bhatti, J. S.: Postfire carbon balance in boreal bogs of Alberta, Canada, Glob. Chang. Biol., 15(1), 63–81, doi:10.1111/j.1365-2486.2008.01756.x, 2009.

Winiger, P., Andersson, A., Eckhardt, S., Stohl, A., Semiletov, I. P., Dudarev, O. V., Charkin, A., Shakhova, N., Klimont, Z., Heyes, C. and Gustafsson, Ö.: Siberian Arctic black carbon sources constrained by model and observation, Proc. Natl. Acad. Sci., 114(7), E1054–E1061, doi:10.1073/pnas.1613401114, 2017.

Winker, D. M., Vaughan, M. A., Omar, A., Hu, Y., Powell, K. A., Liu, Z., Hunt, W. H. and Young, S. A.: Overview of the CALIPSO mission and CALIOP data processing algorithms, J. Atmos. Ocean. Technol., 26(11), 2310–2323, doi:10.1175/2009JTECHA1281.1, 2009.

Wu, D., Huang, X., Norman, F., Verplaetsen, F., Berghmans, J. and Van Den Bulck, E.: Experimental investigation on the self-ignition behaviour of coal dust accumulations in oxy-fuel combustion system, Fuel, 160, 245–254, doi:10.1016/j.fuel.2015.07.050, 2015.

Zhuravleva, T. B., Kabanov, D. M., Nasrtdinov, I. M., Russkova, T. V., Sakerin, S. M., Smirnov, A. and Holben, B. N.: Radiative characteristics of aerosol during extreme fire event over Siberia in summer 2012, Atmos. Meas. Tech., 10(1), 179–198, doi:10.5194/amt-10-179-2017, 2017.

FIGURE LEGENDS

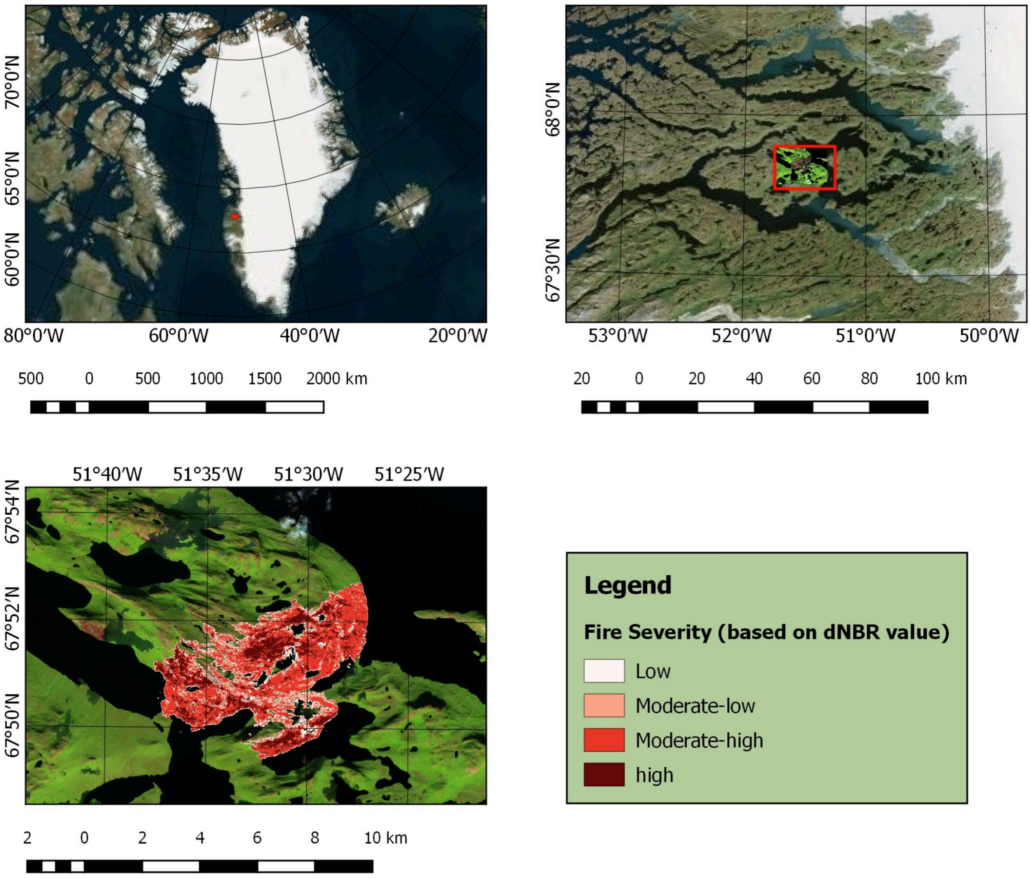

Figure 1. Map of Greenland (upper left) and zoomed map marked with fire location (upper right and burned area classification (bottom) in terms of fire severity according to Sentinel 2A images for fires burning in Greenland in August 2017. To delineate fire perimeters, both Landsat 8 OLI and Sentinel 1A – 2A data were used (**Table 1**).

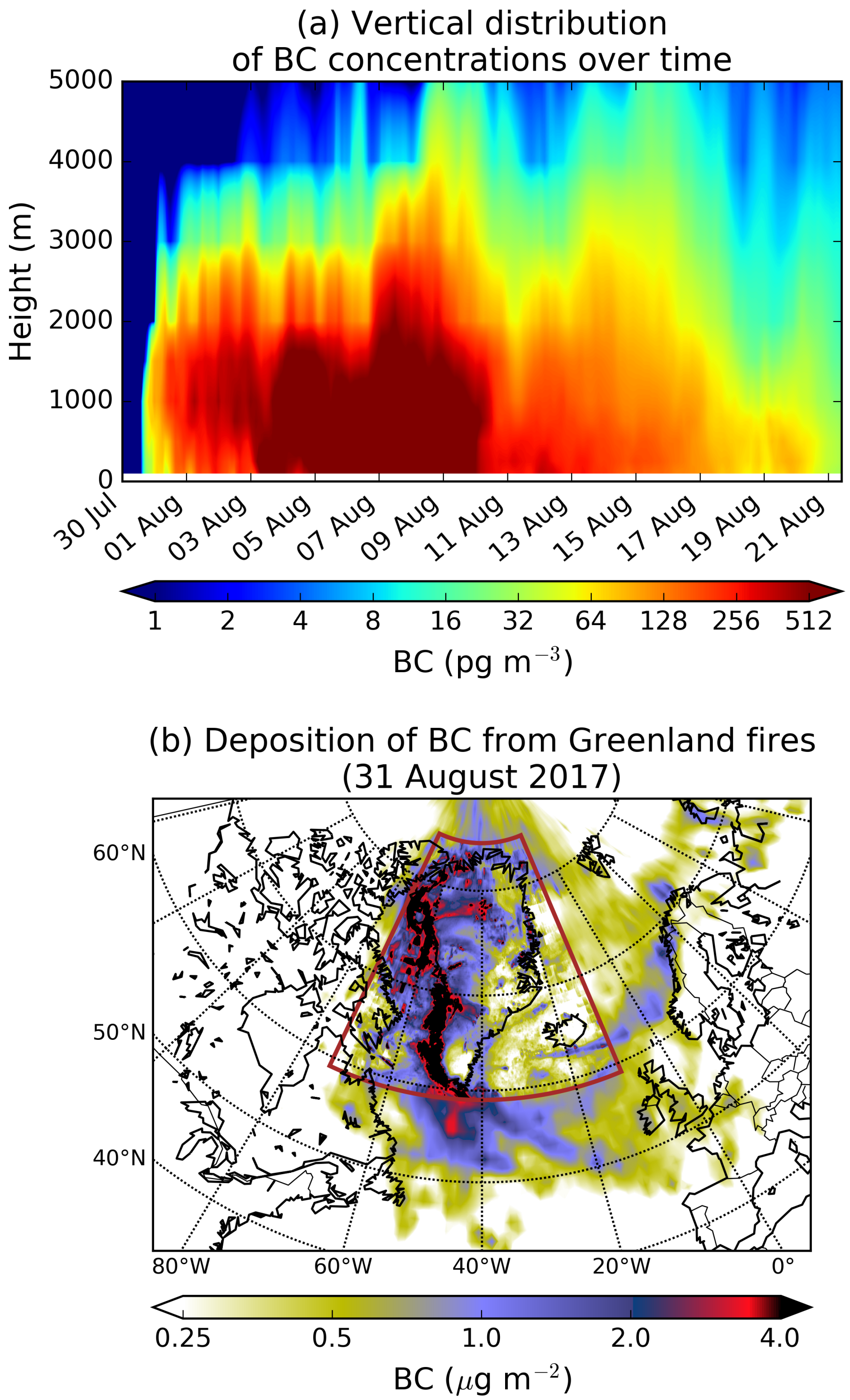

Figure 2. (a) Time-series of vertical distribution of BC concentrations averaged over the area of Greenland in summer 2017 as a function of time. (b) Total (wet and dry) deposition of BC (in μg m^{-2}) from Greenland fires until 31 August 2017. The colored rectangle depicts the nested high-resolution domain.

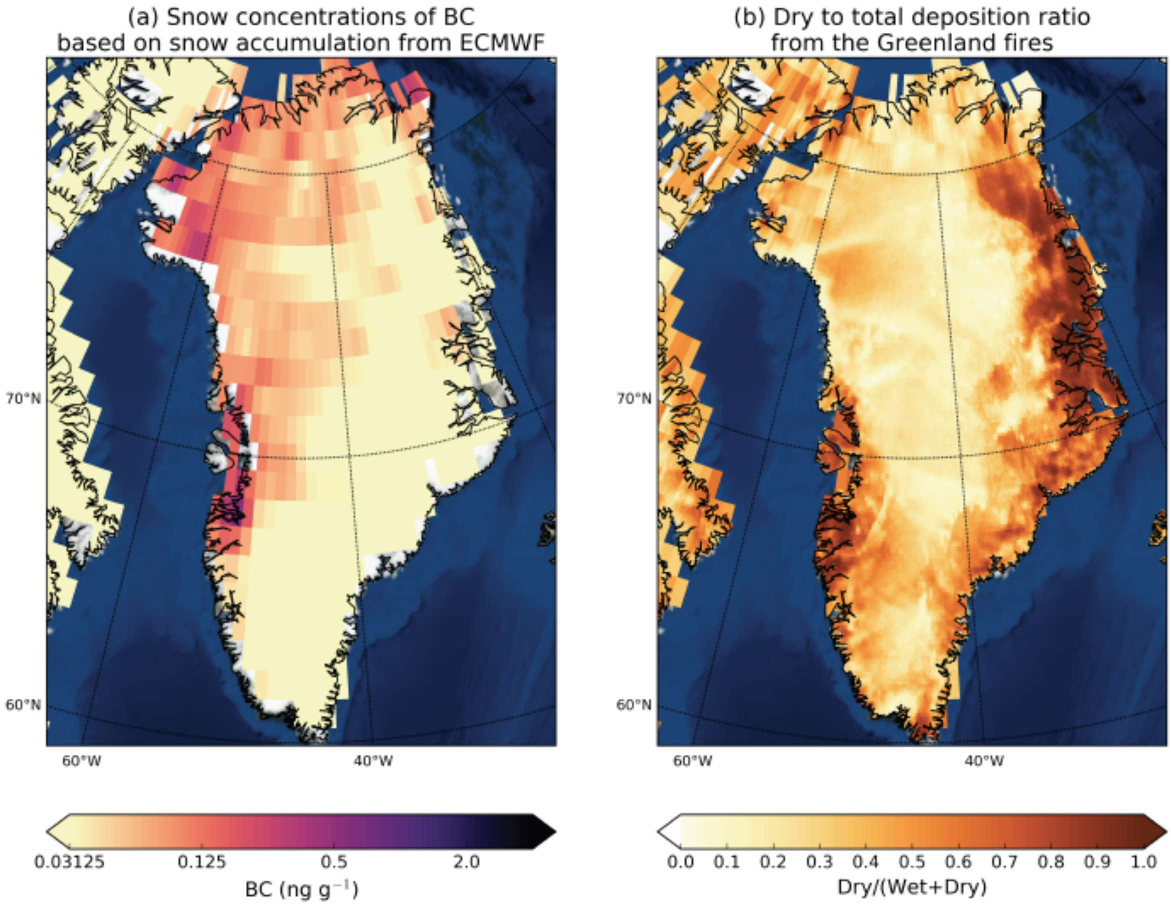

Figure 3. (a) Calculated snow concentrations of BC over Greenland based on the modeled deposition and the snow precipitation (large scale and convective) in the operational ECMWF data that were used in our simulation (see section 2.3). (b) Dry to total deposition ratio of BC from the 2017 peat fires over Greenland.

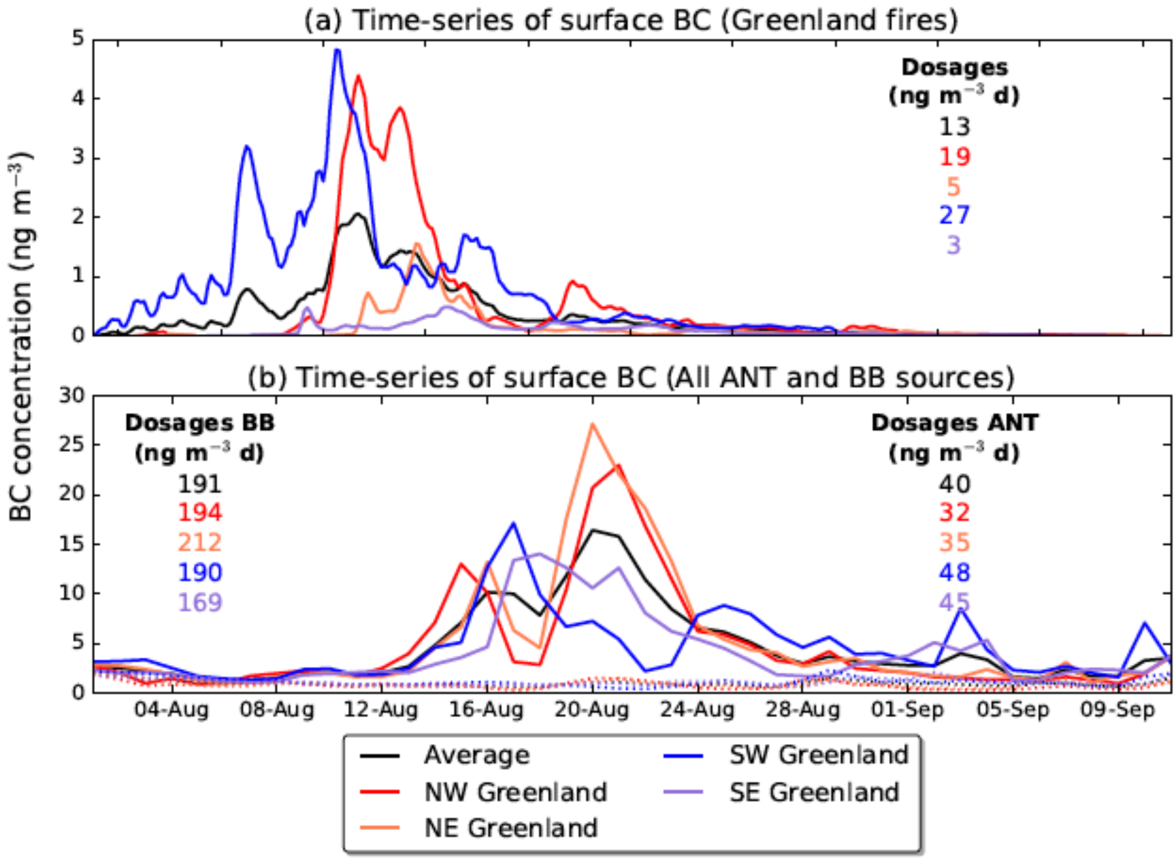

Figure 4. (a) Time-series of surface BC concentrations in Northwestern, Northeastern, Southwestern and Southeastern Greenland from the summer 2017 fires in Western Greenland. (b) Time-series of surface BC concentrations in Northwestern, Northeastern, Southwestern and Southeastern Greenland from global anthropogenic (ANT, dashed lines) and biomass burning (BB, solid lines) emissions for the same period. The numbers represent the respective dosages (time-integrated concentrations) for the time period shown. The color codes are reported in the legend.

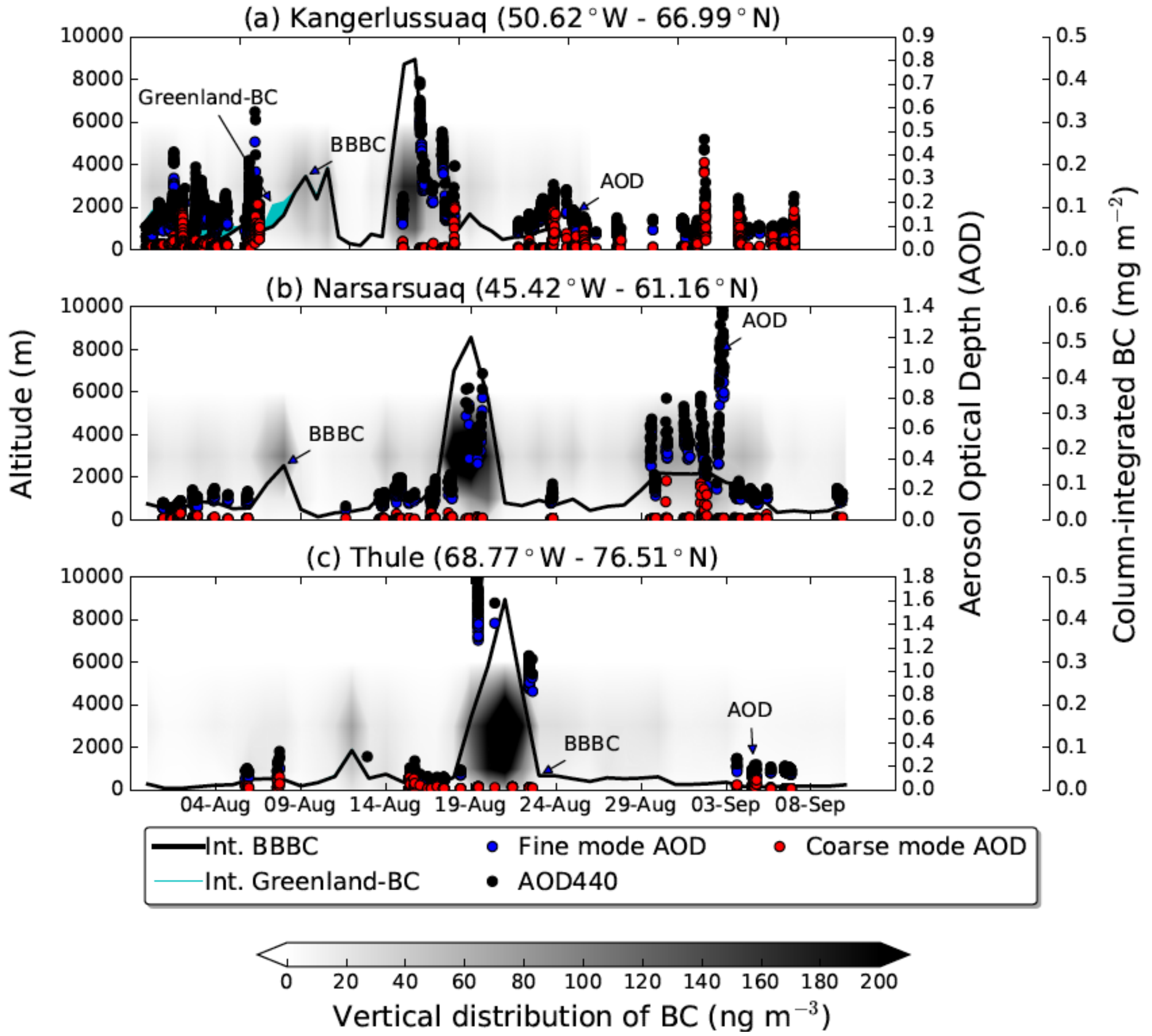

Figure 5. Contour plot of the vertical distribution of simulated BC (altitude a.g.l. shown on left y-axis) as a function of time (x-axis) and time-series of column-integrated simulated BC (extended right axis) from fires burning outside Greenland (black line) and Greenland fires (cyan stacked area). Column-integrated BC from anthropogenic sources was extremely small and it is not plotted here. Time-series for fine (blue) and coarse mode (red) AOD at 500 nm and total AOD at 400 nm (black) correspond to the right y-axis. The three panels show results for stations (a) Kangerlussuaq, (b) Narsarsuaq and (c) Thule (sorted from the closest to the farthest station).

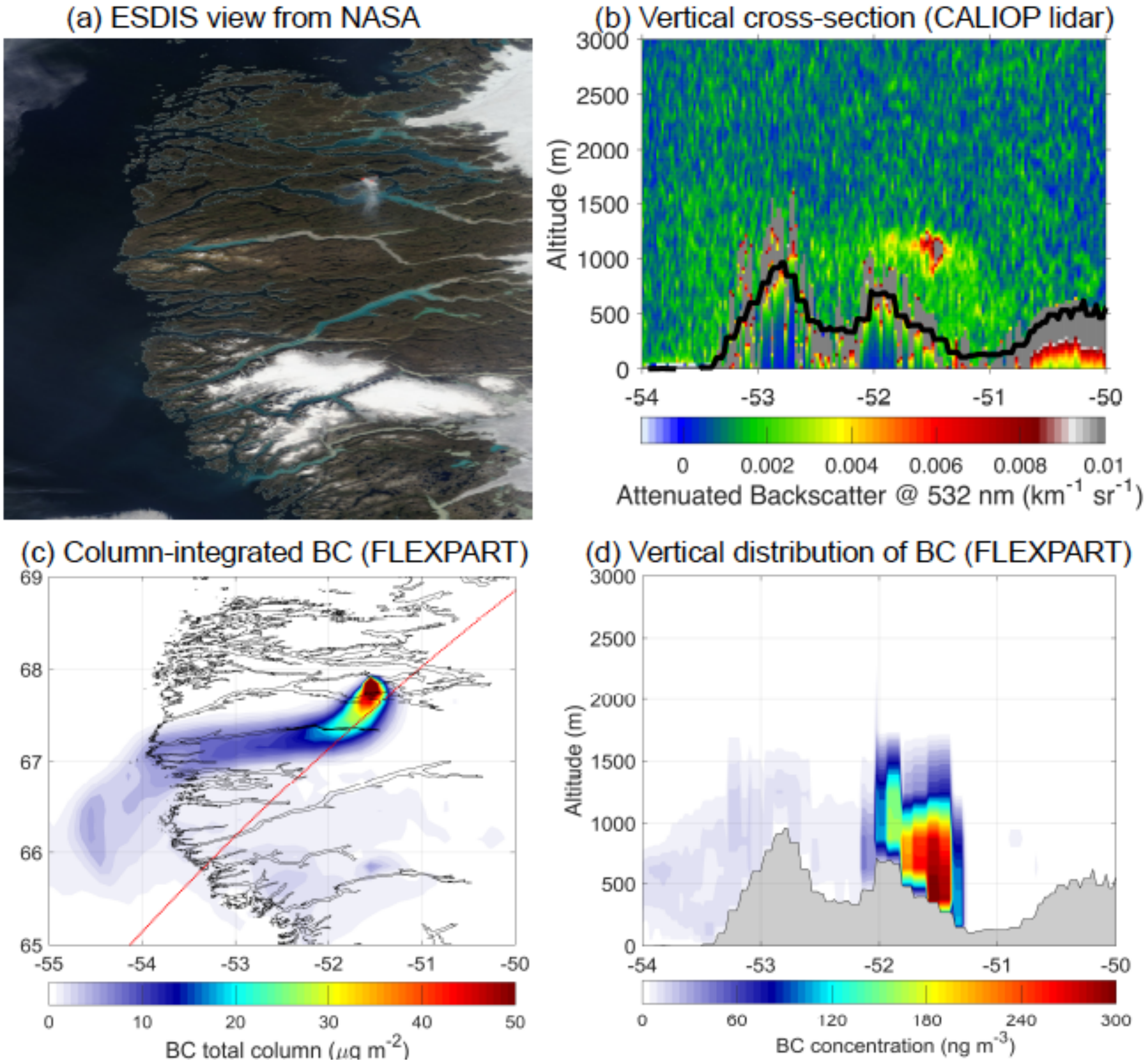

Figure 6. (a) Worldview application from the NASA/Goddard Space Flight Center Earth Science Data and Information System (ESDIS) project on 14 August 2017. (b) Vertical cross-section along satellite's route (red line in c) of total attenuated backscatter at a wavelength of 532 nm obtained from the CALIOP lidar on 14 August 2017 at 6 UTC (black line denotes the orography of the area). (c) Column-integrated BC concentration simulated with FLEXPART (read line shows the path of the satellite). (d) Vertical distribution of BC concentrations with longitude as seen with FLEXPART (grey area denotes the orography of the area).

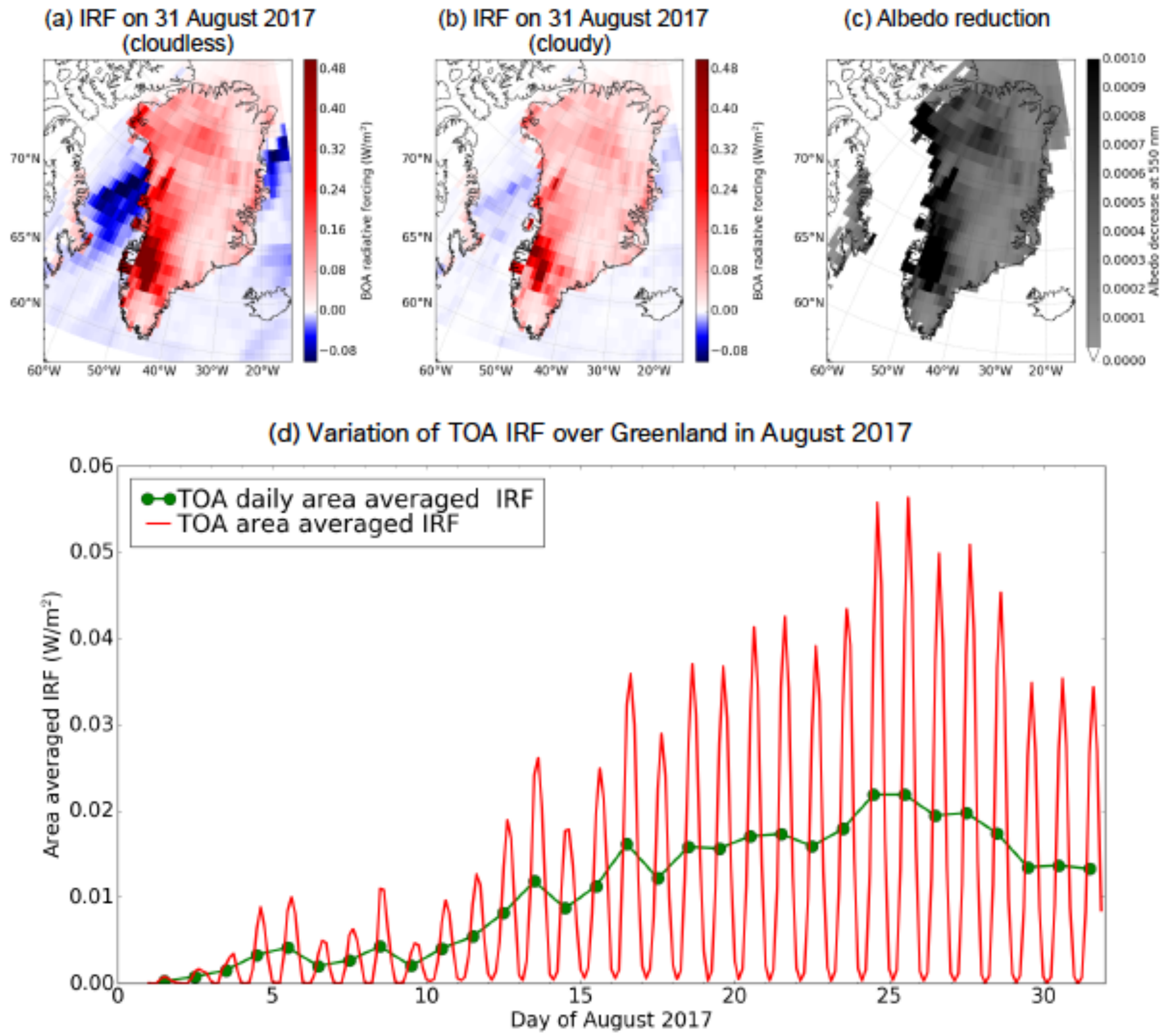

Figure 7. (a) The instantaneous direct BOA RF due to BC from the Greenland fires for cloudless and (b) cloudy conditions on 31 August, and (c) snow albedo reduction due to the total BC deposited as a result of the Greenland fires. (d) Temporal variation of the cloudy TOA IRF over Greenland in August 2017.

SUPPLEMENTARY FIGURE LEGENDS

Figure S 1. Annual number of active fires over Greenland during the last 17 years as seen from NASA's MODIS satellite (product MSC14DL).

Figure S 2. Fire dynamics in Greenland for the August 2017 fires according to MODIS (magenta dots show active fire hot spots from the MODIS MCD14DL product). Locations of stations with AOD measurements from AERONET are also shown.

Figure S 3. Median injection heights (km above sea level – ASL; left panel) and distribution of longitudinally integrated burned biomass (Tg) as a function of injection altitude (right panel) calculated by PRMv2 for the period between 31 July and 21 August 2017.

Figure S 4. Relative standard deviation of BC deposition for different assumed size distributions of BC normalized against the results for our reference size distribution with a logarithmic mean diameter of 0.25 μm. Particle size distributions with aerodynamic mean diameters of 0.1, 0.25, 0.5, 1, 2, 4, 8 μm and a logarithmic standard deviation of 0.3 were simulated.

Figure S 5. Footprint emissions sensitivities for Northwestern, Northeastern, Southwestern and Southeastern Greenland for the period 31 July to 31 August 2017. Active fires from NASA's MODIS MCD14DL product are shown with red dots.

Figure S 6. Average contribution of biomass burning (upper panels) and anthropogenic emissions (lower panels) to surface concentrations of BC in Northwestern, Northeastern, Southwestern and Southeastern Greenland (in ng m^{-3} per grid cell). Numbers (in red) represent total concentrations in the studied domain, obtained by spatial integration over all source grid cells. Receptor areas in Greenland are highlighted by pink boxes.

Figure S 7. (a) The single scattering albedo (SSA) of BC as a function of wavelength for various modified combustion efficiencies (MCE). The star and dot marked lines are from the parameterization of Pokhrel et al. (2016). (b) The IRF as a function of BC deposited on the

Ice Sheet. The calculations were made for cloudless conditions with a snow-covered surface for noon on 31 August 2017 at 65°N.

Table 1. Start and end date of releases, source of data, type of sensor, burned area and daily increment of burned area, fuel consumption and calculated BC emissions from Eq. 1 during the Greenland fires in 2017. Total numbers for burned area, fuel consumption and BC emissions are highlighted in bold.

Start	End	Source of RS data	Type of sensor	Burned area (ha)	Increment of burned area (ha)	Fuel consumption (t C)	BC emission (kg)
31/07/17	02/08/17	Sentinel 2A	MSI	304	304	15176	3035
02/08/17	03/08/17	Landsat 8 OLI	MSI	428	125	6247	1249
03/08/17	04/08/17	Sentinel 1A	SAR	588	160	7980	1596
04/08/17	05/08/17	Sentinel 1A	SAR	740	152	7621	1524
05/08/17	07/08/17	Sentinel 2A	MSI	1100	359	17966	3593
07/08/17	08/08/17	Sentinel 2A	MSI	1314	214	10706	2141
08/08/17	12/08/17	Landsat 8 OLI	MSI	1868	554	27714	5543
12/08/17	14/08/17	Sentinel 1A	SAR	2005	136	6817	1363
14/08/17	15/08/17	Sentinel 1A	SAR	2169	165	8244	1649
15/08/17	16/08/17	Sentinel 1A	SAR	2209	40	1998	400
16/08/17	19/08/17	Sentinel 1A	SAR	2254	44	2213	443
19/08/17	21/08/17	Sentinel 2A	MSI	2345	92	4579	916
TOTAL					**2345**	**117259**	**23452**

RS - Remote Sensing
MSI - Multispectral Images
SAR - Synthetic Aperture RADAR